HHS Public Access

Author manuscript

Exp Eye Res. Author manuscript; available in PMC 2017 September 01.

Published in final edited form as:

Exp Eye Res. 2016 September ; 150: 44–61. doi:10.1016/j.exer.2015.07.016.

Idiopathic preretinal glia in aging and age-related macular degeneration

Malia M. Edwards[a], **D. Scott McLeod**[a], **Imran A. Bhutto**[a], **Mercedes B. Villalonga**[b], **Johanna M. Seddon**[b], and **Gerard A. Lutty**[a]

[a]Department of Ophthalmology, Wilmer Eye Institute, Johns Hopkins Hospital, 400 N. Broadway, Baltimore, Maryland 21287, USA

[b]Ophthalmic Epidemiology and Genetics Service, Department of Ophthalmology, Tufts Medical Center, Tufts University School of Medicine, 800 Washington St #450, Boston, MA 02111 USA

Abstract

During analysis of glia in wholemount aged human retinas, frequent projections onto the vitreal surface of the inner limiting membrane (ILM) were noted. The present study characterized these preretinal glial structures. The amount of glial cells on the vitreal side of the ILM was compared between eyes with age-related macular degeneration (AMD) and age-matched control eyes. Retinal wholemounts were stained for markers of retinal astrocytes and activated Müller cells (glial fibrillary acidic protein, GFAP), Müller cells (vimentin, glutamine synthetase) and microglia/hyalocytes (IBA-1). Retinal vessels were labeled with UEA lectin. Images were collected using a *Zeiss 710* confocal microscope. Retinas were then cryopreserved. Laminin labeling of cryosections determined the location of glial structures in relation to the ILM. All retinas investigated herein had varied amounts of preretinal glial. These glial structures were classified into three groups based on size: sprouts, blooms, and membranes. The simplest of the glial structures observed were focal sprouts of singular GFAP-positive cells or processes on the vitreal surface of the ILM. The intermediate structures observed, glial blooms, were created by multiple cells/processes exiting from a single point and extending along the vitreoretinal surface. The most extensive structures, glial membranes, consisted of compact networks of cells and processes. Preretinal glia were observed in all areas of the retina but they were most prominent over large vessels. While all glial blooms and membranes contained vimentin and GFAP-positive cells, these proteins did not always co-localize. Many areas had no preretinal GFAP but had numerous vimentin only glial sprouts. In double labelled glial sprouts, vimentin staining extended beyond that of GFAP. Hyalocytes and microglia were detected along with glial sprouts, blooms, and membranes. They did not, however, concentrate in the retina below these structures. Cross sectional analysis identified small breaks in the ILM above large retinal vessels through which glial cells exited the retina. Preretinal glial structures of varied sizes are a common occurrence in

Correspondence to: Malia Edwards, PhD, The Wilmer Eye Institute, M023 Smith Building, Johns Hopkins Hospital, 400 North Broadway, Baltimore, Maryland 21287-9115, USA; Tel.: +1 410-614-9888; Fax: +1 410-955-3447; medwar28@jhmi.edu. dmcleod1@jhmi.edu; ibhutto1@jhmi.edu; glutty@jhmi.edu; MVillalonga@tuftsmedicalcenter.org; jseddon@tuftsmedicalcenter.org

aged retinas and, in most cases, are subclinical. While all retinal glia are found in blooms, vimentin labeling suggests that Müller cells form the leading edge. All retinas investigated from eyes with active choroidal neovascularization (CNV) had extensive glial membranes on the vitreal surface of the ILM. Although these structures may be benign, they may exert traction on the retina as they spread along the vitreoretinal interface. In cases with CNV, glial cells in the vitreous could bind intravitreally injected anti-vascular endothelial growth factor. These preretinal glial structures indicate the remodeling of both astrocytes and Müller cells in aged retinas, in particular those with advanced AMD.

Keywords

age-related macular degeneration; astrocytes; epiretinal membranes; Muller cells; glia

1. Introduction

There are two types of macroglia in retina, astrocytes and Müller cells. Astrocytes normally reside only in the nerve fiber layer where they associate closely with retinal blood vessels and ganglion cell axons (Provis et al., 2000). Within the vascular arcades, astrocytes align radially with nerve fibers while they form a chicken wire-like pattern in other areas. Müller cells, radial glia, provide the suprastructure and interact with most retinal cell types. They assume many roles played by astrocytes in the brain, including maintaining ion homeostasis, glutamine synthesis, and assisting in synaptic activity (Reichenbach and Bringmann, 2013). Müller cells also help form the blood retinal barrier (BRB) of the deep retinal vasculature. While Müller cell nuclei are found in the inner nuclear layer, their processes span the entire retina. Müller cell radial processes terminate in the inner retina as endfeet binding the inner limiting membrane (ILM) and in the outer retina at the photoreceptor inner segments, forming the external limiting membrane.

Although often classified as glia, microglia are of monocytic origin. These dendritic cells normally reside in the inner retina but extend into the outer layers and the subretinal space during injury (Huang et al., 2013; Lee et al., 2008). These cells constantly search for changes to the retinal milieu (Wang et al., 2014; Wong, 2013). Upon detecting stimuli, microglia are activated and migrate to sites of injury, releasing cytokines and chemokines.

Glial cells maintain the integrity of the BRB and ILM as well as the vitreoretinal interface. Disruptions to the ILM and/or abnormal migration of glial and vascular cells into the vitreous are common to many retinal diseases, including diabetic retinopathy and retinal detachment (Bringmann and Wiedemann, 2009; Foos, 1972a, 1977; Garweg et al., 2013; Sethi et al., 2005). These migrated cells exert traction on the retina, potentially leading to retinal detachment.

Foos first identified idiopathic preretinal glial projections and simple glial epiretinal membranes (ERMs) over four decades ago using transmission electron microscopy (TEM) (Foos, 1972a, 1974). These projections were found primarily in aged specimens with some form of retinal disease but were occasionally observed in younger retinas (Foos, 1972b, 1974). Glial projections onto the vitreal surface and simple epiretinal membranes were

observed primarily over large retinal vessels and vessel branch points, both areas with an attenuated ILM (Foos, 1977; Pedler, 1961). While Foos elegantly described the ultrastructure of preretinal glial structures using TEM, the technology to identify individual cell types was not yet available.

The present study immunohistochemically characterized preretinal glial projections and membranes similar to those observed by Foos. The occurrence of these glial structures, herein referred to as sprouts, blooms or membranes, was investigated in aged controls and age-related macular degeneration (AMD) wholemount retinas to determine if there was a correlation with this disease state.

2. Methods

2.1 Tissue

Human donor eyes were obtained within 24 hrs postmortem from National Disease Research Interchange (NDRI), Johns Hopkins Hospital Department of Pathology, and from the AMD Registry and Biorepository in collaboration with Dr. Johanna Seddon. The use of tissue was approved by the Institutional Review Board at Johns Hopkins University and Tufts Medical Center. Eyes were collected from 20 AMD patients and eight non-AMD age-matched controls (Table 1). For four donors, both retinas were investigated. Therefore, a total of 32 eyes (22 AMD and 10 non-AMD) were used in this study. Eyes received from the AMD Registry included complete ocular and systemic health histories. Donors ranged in age from 64-102 yrs (average 88 +/− 8 yrs). No donors in this study had a history of victrectomy.

2.2 Classification of AMD disease state

AMD donors were grouped according to disease state based on recent worst clinical diagnosis by the Clinical Age-Related Maculopathy Staging System (CARMS) grading system (Seddon et al., 2006) and pathological examination of the retina and choroid. A recent worst grade of 1 was considered non-AMD while a grade of 2 and/or observations of some drusen was considered early. A recent grade of 3 and/or drusen and pigment abnormalities was classified as intermediate AMD. A recent worst grade of 4 and/or observations of retinal pigment epithelial and choriocapillaris loss were classified as geographic atrophy (GA). Those with a recent worse score of 5B and/or choroidal neovascularization (CNV) noted clinically and pathologically were classified as neovascular AMD.

2.3 Immunohistochemistry of wholemount retinas

The anterior chamber was removed and gross photos were taken of the posterior pole. Retinas were then dissected from the eye cup and fixed overnight at 4 °C in 2% paraformaldehyde in 0.1 M cocadylate buffer. The choroid was imaged with and without retinal pigment epithelial cells to verify clinical AMD grades. Following washes in tris-buffered saline with 0.1% Triton-X100 (TBST), retinas were blocked overnight at 4 °C with 5% goat serum in TBST containing 1% bovine serum albumin (BSA, Pentax Fraction V, Sigma). Wholemounts were divided into pieces (posterior pole, inferior, nasal, temporal and superior) to allow the use of multiple antibodies. Retinas were then incubated with primary

antibodies prepared in TBST with 1% BSA for 72 hrs at 4 °C. After washes, retinas were incubated in secondary antibodies (diluted 1:200) along with Ulex europas agglutinin (UEA) lectin tagged with FITC (Sigma; 1:100) for 48 hrs at 4°C. After washes in TBST, retinas were UEA (stored in TBS with 0.2% sodium azide until imaged. Choroids were also stained with UEA lectin to identify any vessel loss or CNV. Antibodies used are listed in Table 2.

2.4 Cross sectional analysis of wholemounts

After retinas were imaged as wholemounts, they were cryopreserved with a sucrose gradient as previously described (Edwards et al., 2011). Retinas were then infiltrated with 20% sucrose: Optimal Cutting Temperature (OCT; Tissuetek) solution (2:1) for 30 min and frozen. Eight micron sections were cut on a *Leica* cryostat. Sections were either imaged with only original labels or stained with additional antibodies as previously described (Edwards et al., 2011). Primary antibodies used on cross sections included: rabbit anti-pan laminin (Sigma, 1:200) and chick anti-vimentin (Millipore, 1:500). Sections were exposed to primary antibody for 2 hrs at RT and to secondary antibody (1:500) for 30 min.

2.5 Imaging

Confocal Z stack images were acquired using a *Zeiss* 710 confocal microscope and Zen software (*Carl Zeiss*). Large 5 × 5 tiled Z stacks were collected at 5x and 10x using GFAP staining as the top focal plane and UEA-lectin for the bottom focal plane. Tiled images in the posterior pole were collected at 2048 × 2048 pixel resolution while those in the other regions were collected at 1024 × 1024 pixel resolution. High resolution (2048 × 2048) images were collected at higher magnifications. For 3D rendering, images were collected at 12 bit with the optimal slice settings (for 20x this was 50-70 0.72-1.0 μm slices). *Imaris* software (Bitplane) was used for image analysis and 3D rendering.

2.6 Calculation of glial bloom areas

Tiled 5x and 10x Z-stacks were flattened and stitched to create tissue maps. The 10x objective images were used to calculate the percent of the ILM covered by glial cells/processes for each retinal piece (Fig. 1A). These tiled images covered a 3.8 × 3.8 mm^2 piece of the retina. Preretinal glial projections could easily be distinguished by their focal plane because they overlay the astrocytes in the retina and were more intensely labeled. The magic wand, with the anti-alias and contiguous selected, and/or lasso tools were used to select preretinal $GFAP^+$ cells and processes. The tolerance was set between 15 and 30 depending on the size of the glial structure (smaller projections required a lower tolerance to avoid selecting retinal astrocytes). Once all preretinal glial cells and processes were selected, these were copied and placed into a new Tiff image (Fig. 1B). The new image was opened in *Image J* (NIH) and made binary. The percentage of the ILM covered by preretinal glial cells was determined using the percent black to white ratio macro. T-tests were performed to compare the percentage in retinas with different stages of AMD to that of non-AMD retinas.

2.7 JB-4 analysis and staining

Select areas of retina were fixed flat in quarter strength Karnovsky's glutaraldehyde/paraformaldehyde, dehydrated, embedded flat in polyacrylamide (JB4, Polysciences) as

published previously (McLeod et al., 1995). Sections were stained with either toluidine blue or Periodic-Acid Schiff (PAS) and hematoxylin.

3.0 Results

All retinas investigated contained preretinal GFAP$^+$ glia. These glial cells created structures that were divided into three classifications based on their size. The following sections will describe the different preretinal glial structures.

3.1 Glial sprouts

Glial sprouts, the simplest preretinal glial structures, were observed in all retinas. At low magnification, these appeared to be single processes that extended through the ILM (Fig 2A). Closer examination revealed that a large portion of or entire cell bodies were on the vitreal side of the ILM (Fig. 2B, D, G, J). Glial processes in sprouts were thicker with more intense GFAP staining compared to astrocytes in the retina. Some sprouts extended linearly between 100-200 μm from the point at which they exited the retina (Fig. 2B, D, G, L). Others had a stellate morphology with multiple processes, resembling astrocytes (Fig. 2B, J, L). Sprouts often terminated in arborizations of multiple fine processes. These fine processes extended into the retina and/or connected with other sprouts (Fig. 2B, D, G-I, L; Supplemental Fig. 1). Deeper focal planes show the exit point of glial sprouts (Fig. 2E). The overall astrocyte pattern was normal below sprouts but tangles and/or skewed GFAP$^+$ processes were often noted where glia exited the retina (Fig. 2C, F, K).

3.2 Glial blooms

Multiple GFAP$^+$ processes extending along the vitreoretinal surface in one focal area created glial blooms (Fig. 3). Glial blooms extended 200- 800 μm from their exit point along the vitreoretinal surface (Fig. 3A, B). Many blooms were connected by individual glial processes (Fig. 3B). Neighboring glial sprouts that coalesced within the vitreous created a dense cluster of GFAP$^+$ processes, one form of glial blooms (Fig. 3C). The majority of blooms were created by multiple glial processes fanning out from a single main exit point and extending along the vitreoretinal surface, creating a “flower-like appearance” (Fig. 3D, H, J, L). Single glial cell processes traversed as far as 200 μm from their exit point. These thick glial stalks arborized into numerous smaller processes with multiple connections to other preretinal glial cells or retinal astrocytes (Fig. 3E, K). As a result, a net-like structure was frequently observed at the outer edge of blooms (Fig. 3E, F, K). Under preretinal glial blooms, astrocytes maintained a normal pattern (Fig. 3G). GFAP$^+$ processes exiting the retina and extending along the vitreal surface were visible in digital cross sections (Fig. 3I, J).

3.3 Glial membranes

For the purpose of this study, a glial membrane was defined as a dense mat-like structure of GFAP$^+$ cells and processes on the vitreal side of the ILM (Fig. 4). These structures extended greater than 500 μm in all directions along the vitreoretinal surface. In many cases, over 50% of the 3mm^2 retinal piece was covered by a preretinal glial membrane (Fig. 4A). In a few cases, the membrane covered the entire expanse of retina analyzed (Fig. 4B). When the

membrane did not cover the entire area, multiple blooms could be seen coalescing (Fig. 4C). The cells and processes in membranes overlapped with one another more than those in glial blooms, creating a multi-layered structure (Fig. 4D, E, G, H, I, J). In some cases, disorganized processes were observed above the astrocyte processes within the retina (Fig. 4F). Thick, preretinal GFAP$^+$ processes divided into multiple fine branches that made contact with other cells or processes within the vitreous, adding to the complexity of membranes (Fig. 4G). These cells extended processes toward the retina below and made multiple connections with other membrane cells (Fig. 4H).

3.4 Preretinal glia were predominantly found above retinal vessels

While glial sprouts were observed over both large and small vessels, blooms were prominent above larger vessels (especially major arcades vessels), vessel branch points, and areas of artery-vein crossings (Fig. 5). Multiple blooms were frequently observed interconnected along the same retinal vessels. Large membranes were most often found over large arcade vessels. No preretinal vessels were observed.

3.5 Glial structures were on the vitreal surface of the ILM

Retinas with GFAP labeling were sectioned and stained with anti-pan laminin to verify the location of glia in relation to the ILM (Fig. 6A). As expected, astrocytes expressing GFAP were noted below the laminin$^+$ ILM. In many retinas, particularly those with neovascular AMD, Müller cells also expressed GFAP. Above some large retinal vessels, GFAP$^+$ cells/processes projected through breaks in the laminin$^+$ ILM and extending along the vitreoretinal surface.

JB-4 sections verified that glial cells and processes were on the vitreal surface of the ILM (Fig. 6B, C). Breaks in the ILM with glial cells protruding through into the vitreous were observed over large retinal vessels (Fig. 6B). Nuclei were also observed on the vitreoretinal surface (Fig. 6C).

3.6 Both astrocytes and Müller cells exited the retina

In order to distinguish activated Müller cells from astrocytes, vimentin and glutamine synthetase (GS), Müller cell markers, were used along with GFAP. Preretinal glial structures contained both vimentin and GFAP (Fig 7). GFAP and vimentin did not, however, always co-localize. In glial sprouts, vimentin$^+$ cells and processes covered a larger surface area while GFAP-only cells and processes were more linear (Fig. 7A-C). The thick glial processes sprouting from the retina to create glial blooms contained both vimentin and GFAP (Fig. 7D-F). Preretinal cells surrounding glial blooms to create membranes also contained a combination of GFAP only, double-positive, and vimentin-only cells/processes (Fig. 7G-I). Analysis of retinal cross sections further demonstrated the double layer of glial cells (Fig. 7J-L).

Preretinal glial structures also expressed GS but this was largely distinct from that of GFAP (Fig. 8). In some areas, GFAP$^+$/GS$^-$ glial sprouts were surrounded by smaller GFAP$^-$/GS$^+$ sprouts (Fig. 8A-C). Other blooms contained a few GS$^+$ processes/cells amongst numerous GFAP$^+$ cells (Fig. 8D-F). In these areas, GS$^+$ endfeet were missing below blooms (Fig. 8C,

F). When present in blooms, GS was most prominent at the base and did not extend into the longer processes or was much lighter in these areas (Fig. 8D, F, G, I). In some membranes, GFAP$^+$, compact cells were observed adjacent to endfeet with intense GS staining (Fig. 8J-L).

3.7 Müller cells exited the retina ahead of astrocytes

Many retinas contained large areas without preretinal GFAP$^+$ projections (Fig. 9A, B, D, E, G, H). These same areas, however, contained numerous vimetin$^+$ glial sprouts and/or blooms (Fig. 9A, C, B, F, G, I, J, L). These vimentin only sprouts were found most often, but not exclusively, above retinal vessels. Astrocyte processes below these vimentin-only sprouts usually maintained a normal pattern (Fig. 9E, H). In some cases, however, GFAP$^+$ processes appeared tangled (Fig. 9B, K).

Some retinal regions were stained for GS, vimentin, and GFAP to verify that vimentin-positive cells/processes were Müller cells (Supplemental Fig. 2). Numerous sprouts, double positive for vimentin and GS, were noted above retinal vessels in areas without preretinal GFAP. Retinas also contained many “hot spots” with intense staining for GS and vimentin.

3.8 IBA-1$^+$ cells were also associated with preretinal glia

Microglia and hyalocytes, labeled with IBA-1, were associated with glial sprouts, blooms, and membranes (Fig. 10). These cells were not, however, concentrated in the retina where glial cells exited. IBA-1$^+$ cells were most numerous in blooms and membranes.

3.9 The number and size of preretinal glial structures increased with AMD progression

Seven of the ten non-AMD retinas investigated had only glial sprouts throughout the retina (Fig. 11A). Another retina contained numerous glial blooms. The remaining two non-AMD retinas (from the same donor) had multiple blooms along the major retinal vessel arcades which coalesced to form membranes in regions outside the posterior pole. These membranes were observed throughout the retina.

All three retinas with early AMD (from two donors) had glial sprouts in the posterior pole (Fig. 11B). While two of these retinas also had glial sprouts in the temporal and nasal retina, the other had blooms throughout the retina. Glial sprouts were observed throughout two of five retinas with intermediate AMD. The other three intermediate AMD retinas had pan-retinal glial blooms. In one of these retinas, glial blooms expanded to membranes in all retinal regions. Two of the three retinas with GA had glial blooms throughout the retina (Fig. 11C). The other GA retina had numerous glial sprouts in the pole as well as other retinal regions. The blooms in the GA retinas were more numerous than those observed in the non-AMD and early AMD retinas.

In all 11 retinas from eyes with CNV that were imaged in the posterior pole, large glial blooms coalesced to form membranes and covered a majority of the posterior pole (Fig. 11D). In nine of these retinas, these membranes extended in either direction from the retinal arcade vessels. The other two retinas had large glial membranes on the arcades but these were not as prominent in the parafoveal region. A reduction in GFAP$^+$ astrocytes was also

noted in these two retinas. In all but two cases of neovascular AMD, membranes were confined to the posterior pole or areas surrounding the arcades. Other retinal regions had only glial sprouts or isolated blooms.

The percentage of each retinal piece covered by preretinal $GFAP^+$ glia was calculated (Fig. 11E). An average of 3.8 (+/− 5.1) % of the ILM in the posterior pole was covered by preretinal $GFAP^+$ cells and processes in the non-AMD retinas. This percentage was slightly lower in the early AMD retinas at 2.9 (+/−0.8%). The average increased to 4.4 (+/−4.6) % in the intermediate AMD retinas. While not significant, there was a slight increase to 6.6 (+/−2.1) % in the GA group. In the neovascular AMD cohort, the percent increased significantly to 36 (+/− 21) % ($p<0.005$). There was no difference in the percentage outside the posterior pole between any disease groups. Less than 2% of the ILM was covered with preretinal glia in all groups outside the posterior pole. Within the neovascular AMD group, retinas receiving no treatment were compared to those receiving either anti-VEGF or laser (Supplemental Fig. 3). While this difference did not reach significance, the percentage was lower in retinas that had not received treatment. There was no correlation between the amount of preretinal glia and reduced visual acuity.

4.0 Discussion

The present report expanded on the elegant TEM studies of Foos and colleagues which demonstrated idiopathic glial projections onto the vitreal side of the ILM in aged human retinas (Foos, 1972a, b, 1974, 1977). Preretinal glial structures of various degrees were noted in all retinas investigated herein. Using immunohistochemistry, both astrocytes and Müller cells were identified in these structures. The frequent observation of $GFAP^-$, $vimentin^+$ or $GFAP^-$, GS^+ glial sprouts suggests that Müller cells exit the retina ahead of astrocytes. This finding is not surprising given that Müller cell endfeet bind the ILM. Furthermore, the ILM provides guidance to Müller cell processes during development (Halfter et al., 2001). Müller cells also lead epiretinal membrane formation following retinal detachment (Fisher and Lewis, 2003; Fisher et al., 2005).

Although Müller cells were at the vanguard of the preretinal glial formations documented herein, the expression of GS by preretinal Müller cells varied. While some glial blooms had GS throughout, the expression of this protein was strongest at the base of preretinal glial structures. This observation may reflect the compartmentalized protein expression by Müller cells. GS is not needed on the vitreoretinal surface so its expression here is reduced. Alternatively, GS expression by preretinal Müller cells may reflect changes to this protein within the retina. Müller cell GS expression has been shown to decrease in response to retinal remodeling (Lewis et al., 1994). GS expression could also be reduced in response to AMD or aging. Investigation of Müller cell GS expression within the retina is currently underway.

As was observed by Foos, preretinal glia were found predominantly above large retinal vessels, vessel branch points, or arterial-venous crossing (Foos, 1972a). The major retinal vessel arcades contained the most glial membranes. These vascular areas are all areas where the ILM is known to be attenuated (Foos, 1977; Pedler, 1961). Interestingly, the ILM is also

much thinner surrounding the optic disc where glial cells were also observed on the vitreal surface of the ILM (data not shown). Glial blooms and sprouts were observed away from retinal vessels, indicating that other areas of ILM attenuation exist throughout the aged human retina or other factors, such as changes to the retinal milieu, cause glial cells to exit the retina.

The presence of Müller cell only sprouts and astrocyte/Müller cell sprouts throughout all aged human retinas suggests that these cells normally send small processes through the ILM. In many cases, however, multiple processes exited the retina and glial cells extended further along the vitreoretinal surface to create blooms and membranes. The question then arises, what causes a glial sprout to expand to a bloom or membrane? The medical and ophthalmic history of donors was reviewed to identify any factors that correlated with increased glial blooms and membranes. Donors with diabetes or vascular disease often, but not always, had large glial blooms and membranes throughout the retina. These variations may reflect differences in compliance with diet and medication or the duration of diabetes. Five donors within this study cohort suffered from glaucoma. Retinas from four of these five donors had large blooms and membranes and one had only glial sprouts. Interestingly, the four retinas with membranes were from eyes that also had CNV while the other had early AMD. A significant correlation was found between AMD severity and increased preretinal glia. Glial blooms were more prominent in retinas with intermediate AMD compared to those without AMD. Although not significant, there was a slight increase in the amount of preretinal glia in retinas from donors with GA. A significant increase in preretinal glial membranes was found in eyes with CNV compared to those with either no or less advanced AMD. This is consistent with a previous study that reported preretinal glial membranes in AMD retinas (Ramirez et al., 2001). That study did not, however, observe any preretinal glia in control retinas. These authors likely looked only at structures which were defined as glial membranes in the present study.

Clinical studies have also observed an association between epiretinal membrane (ERM) formation and neovascular AMD (Krebs et al., 2007; Lee et al., 2009). Clinical history was accessible for most retinas reported herein. While twelve retinas investigated had extensive preretinal glial membranes, only two had ERMs that were detected by OCT. Review of recent OCT data revealed a potential ERM in one patient that was not noted in clinical observations. Therefore, many of the preretinal glial structures observed herein were subclinical, suggesting that a greater association may exist between ERMs and AMD than is currently reported. The presence of subclinical glial membranes could be important when treating AMD patients because astrocytes and Müller cells, which both express VEGF, may prevent therapies from reaching their target in the outer retina. Indeed, one study reported that vitrectomy improved the response to VEGF therapy in patients with vitreoretinal traction (Mojana et al., 2008). A recent study also demonsrated that atrophy following anti-VEGF therapy grew faster in eyes with epiretinal membranes (Grunwald et al., 2015). Astrocytes have VEGF receptors and increase expression of these receptors in response to injury (Koyama et al., 2011; Koyama et al., 2014; Krum et al., 2008; Krum and Rosenstein, 1998). Given that the subclinical glial structures noted herein may progress to clinically significant membranes, preventing glial membrane formation could improve treatment of

AMD. Therefore, it is important to understand how simple glial sprouts progress to extensive membranes.

Interestingly, the vitreous attachment sites are greatest in the areas containing the most glial blooms (Sebag, 1992; Spencer and Foos, 1970). This observation suggests that interactions with the vitreous may stimulate glial cell migration. Indeed, intravitreal injections of basic fibroblast growth factor stimulate glial migration into the feline vitreous (Lewis and Fisher, 2003). The vitreous liquefies after age 50, altering the components of this structure (Sebag, 1989, 1992). The amount of hyaluronic acid, a stimuli of glial cell migration, increases in the vitreous with age (Sebag, 1989). Furthermore, both Müller cells and astrocytes express CD44, a receptor for hylauronic acid. CD44 is upregulated in response to photoreceptor damage (Kuhrt et al., 1997). These data suggest that preretinal glial membranes would increase with age. While no young donors were included in this study cohort, the youngest donor (64 yr) had very few isolated glial sprouts. Foos also reported that preretinal glial projections and membranes were primarily seen in aged, diseased retinas (Foos, 1972a, b, 1974, 1977). A recent study used proteomics to determine the vitreal changes associated with neovascular AMD (Koss et al., 2014). Two of 19 proteins identified to be upregulated in AMD were fibrinogen and prostaglandin H2-D isomerase. Interestingly, these are both increased in diabetic retinopathy (Garcia-Ramirez et al., 2007; Kim and Franses, 2006). Fibrinogen and prostaglandin stimulate astrocyte scar formation and migration respectively (Schachtrup et al., 2010; Suk, 2012).

While the vitreous may contain stimuli for glial migration and proliferation, an association has been shown between posterior vitreous detachment and ERM formation (Foos, 1977; Wiznia, 1986). Therefore, the normal vitreous may actually contain factors which inhibit glial migration (Gass, 1988). When the vitreal components are altered, degraded, or separated from the retina, these factors may be lost and the glial cells in areas of strong vitreoretinal adhesion migrate into the vitreous. As noted above, the vitreous is also altered in AMD and factors inhibiting glial migration could be reduced.

Retinal changes, such as inflammation, may also stimulate glial cell proliferation and/or migration along the vitreoretinal surface. This idea is supported by the fact that, in 83% of retinas with neovascular AMD, glial membranes were confined to the affected area, posterior pole. Inflammation and oxidative stress have been implicated in the pathology of both AMD and diabetic retinopathy (Blasiak et al., 2013). As has been previously published, Müller cells were activated ($GFAP^+$) in most retinas investigated herein with neovascular AMD (Sullivan et al., 2003; Wu et al., 2003). It would be interesting to determine if preretinal glial blooms and membranes are found throughout retinas with other retinal degenerations. If so, glial membranes could reflect remodeling of Müller cells in response to photoreceptor loss. Retinal remodeling and preretinal glial membrane formation has also been observed in response to retinal detachment and reattachment (Charteris et al., 2002; Fisher et al., 2005).

Another explanation for the expansion of glial cells on the vitreoretinal surface is that the ILM components stimulate glial cell migration and proliferation. Indeed, these proteins stimulate astrocyte and Müller cell migration during development (Gnanaguru et al., 2013;

Halfter et al., 2001). Changes to the ILM in AMD retinas may provide an attractive matrix on which to migrate. Support for the ILM's role in glial bloom formation lies in a retrospective study showing reduced recurrence of ERMs with ILM peeling (Kwok et al., 2005). Similarly, ILM peeling reduced macular hole recurrence, most likely due to the removal of vitreoretinal traction (Wang et al., 2009; Yoshida and Kishi, 2007).

An important observation made during this study was the reduction in astrocytes in the macula of two retinas with CNV (data not shown). This reduction was associated with fewer membranes in the parafoveal region despite large membranes on the arcades. While not yet fully investigated, at least one case had a submacular glial scar. This suggests the possible remodeling of retinal glia during AMD and in response to AMD treatments. Although beyond the scope of this study, ganglion cell nerve fibers were also observed within preretinal glial structures (unpublished data). Further research is underway to determine the neuroglial interactions involved in preretinal glial membrane formation. Future studies will also be aimed to fully understand these changes and their impact on AMD pathology.

5. Conclusion

Müller cells extend processes into the vitreous when encountering areas of ILM attenuation. Stimuli in the vitreous or glial activation within the retina cause these cells to migrate along the vitreoretinal surface. These cells appear to proliferate and recruit other cells, including astrocytes, from the retina. While the factors responsible for glial membrane formation have yet to be identified, glial blooms and membranes were seen more frequently in retinas with active CNV. Therefore, preretinal glial membrane formation may indicate glial remodeling in neovascular AMD. This remodeling could affect the efficacy of intravitreal treatments.

Supplementary Material

Refer to Web version on PubMed Central for supplementary material.

Acknowledgements

This research was supported by funding from the NEI/NIH EY009357, EY016151 (GL) and EY01765 (Wilmer), NEI/NIH EY013309 (JMS), RPB (Wilmer and Tufts), Tufts Macular Degeneration Research Fund (JMS), and the Beckman Foundation (GL and JS). The authors are grateful to Charles Eberhart, M.D. and Rachel E. Silver, MPH for assistance with acquisition of postmortem eyes. The authors also wish to thank Adam Wenick, M.D., PhD for discussion and assistance with clinical interpretation. Finally, the authors are deeply indebted to the eye donors and their families for making this study possible.

References

Blasiak J, Salminen A, Kaarniranta K. Potential of epigenetic mechanisms in AMD pathology. Front Biosci (Schol Ed). 2013; 5:412–425. [PubMed: 23277059]

Bringmann A, Wiedemann P. Involvement of Muller glial cells in epiretinal membrane formation. Graefes Arch Clin Exp Ophthalmol. 2009; 247:865–883. [PubMed: 19415318]

Charteris DG, Sethi CS, Lewis GP, Fisher SK. Proliferative vitreoretinopathy-developments in adjunctive treatment and retinal pathology. Eye. 2002; 16:369–374. [PubMed: 12101443]

Edwards MM, McLeod DS, Grebe R, Heng C, Lefebvre O, Lutty GA. Lama1 mutations lead to vitreoretinal blood vessel formation, persistence of fetal vasculature, and epiretinal membrane formation in mice. BMC Dev Biol. 2011; 11:60. [PubMed: 21999428]

Fisher SK, Lewis GP. Muller cell and neuronal remodeling in retinal detachment and reattachment and their potential consequences for visual recovery: a review and reconsideration of recent data. Vision Res. 2003; 43:887–897. [PubMed: 12668058]

Fisher SK, Lewis GP, Linberg KA, Verardo MR. Cellular remodeling in mammalian retina: results from studies of experimental retinal detachment. Progress in retinal and eye research. 2005; 24:395–431. [PubMed: 15708835]

Foos RY. Posterior vitreous detachment. Transactions - American Academy of Ophthalmology and Otolaryngology. American Academy of Ophthalmology and Otolaryngology. 1972a; 76:480–497.

Foos RY. Vitreoretinal juncture; topographical variations. Investigative ophthalmology. 1972b; 11:801–808. [PubMed: 4561129]

Foos RY. Vitreoretinal juncture--simple epiretinal membranes. Albrecht Von Graefes Arch Klin Exp Ophthalmol. 1974; 189:231–250. [PubMed: 4365862]

Foos RY. Vitreoretinal juncture; epiretinal membranes and vitreous. Invest Ophthalmol Vis Sci. 1977; 16:416–422. [PubMed: 852943]

Garcia-Ramirez M, Canals F, Hernandez C, Colome N, Ferrer C, Carrasco E, Garcia-Arumi J, Simo R. Proteomic analysis of human vitreous fluid by fluorescence-based difference gel electrophoresis (DIGE): a new strategy for identifying potential candidates in the pathogenesis of proliferative diabetic retinopathy. Diabetologia. 2007; 50:1294–1303. [PubMed: 17380318]

Garweg JG, Tappeiner C, Halberstadt M. Pathophysiology of proliferative vitreoretinopathy in retinal detachment. Survey of ophthalmology. 2013; 58:321–329. [PubMed: 23642514]

Gass JD. Idiopathic senile macular hole. Its early stages and pathogenesis. Arch Ophthalmol. 1988; 106:629–639. [PubMed: 3358729]

Gnanaguru G, Bachay G, Biswas S, Pinzon-Duarte G, Hunter DD, Brunken WJ. Laminins containing the beta2 and gamma3 chains regulate astrocyte migration and angiogenesis in the retina. Development. 2013; 140:2050–2060. [PubMed: 23571221]

Grunwald JE, Pistilli M, Ying GS, Maguire MG, Daniel E, Martin DF, Comparison of Age-related Macular Degeneration Treatments Trials Research, G. Growth of geographic atrophy in the comparison of age-related macular degeneration treatments trials. Ophthalmology. 2015; 122:809–816. [PubMed: 25542520]

Halfter W, Dong S, Balasubramani M, Bier ME. Temporary disruption of the retinal basal lamina and its effect on retinal histogenesis. Developmental biology. 2001; 238:79–96. [PubMed: 11783995]

Huang H, Parlier R, Shen JK, Lutty GA, Vinores SA. VEGF receptor blockade markedly reduces retinal microglia/macrophage infiltration into laser-induced CNV. PLoS One. 2013; 8:e71808. [PubMed: 23977149]

Kim SH, Franses EI. Competitive adsorption of fibrinogen and dipalmitoylphosphatidylcholine at the air/aqueous interface. Journal of colloid and interface science. 2006; 295:84–92. [PubMed: 16115641]

Koss MJ, Hoffmann J, Nguyen N, Pfister M, Mischak H, Mullen W, Husi H, Rejdak R, Koch F, Jankowski J, Krueger K, Bertelmann T, Klein J, Schanstra JP, Siwy J. Proteomics of vitreous humor of patients with exudative age-related macular degeneration. PLoS One. 2014; 9:e96895. [PubMed: 24828575]

Koyama T, Hackl F, Aflaki P, Bergmann J, Zuhaili B, Waisbren E, Govindarajulu U, Yao F, Eriksson E. A new technique of ex vivo gene delivery of VEGF to wounds using genetically modified skin particles promotes wound angiogenesis. Journal of the American College of Surgeons. 2011; 212:340–348. [PubMed: 21247781]

Koyama Y, Hayashi M, Nagae R, Tokuyama S, Konishi T. Endothelin-1 increases the expression of VEGF-R1/Flt-1 receptors in rat cultured astrocytes through ETB receptors. J Neurochem. 2014; 130:759–769. [PubMed: 24862165]

Krebs I, Brannath W, Glittenberg C, Zeiler F, Sebag J, Binder S. Posterior vitreomacular adhesion: a potential risk factor for exudative age-related macular degeneration? American journal of ophthalmology. 2007; 144:741–746. [PubMed: 17884003]

Krum JM, Mani N, Rosenstein JM. Roles of the endogenous VEGF receptors flt-1 and flk-1 in astroglial and vascular remodeling after brain injury. Exp Neurol. 2008; 212:108–117. [PubMed: 18482723]

Krum JM, Rosenstein JM. VEGF mRNA and its receptor flt-1 are expressed in reactive astrocytes following neural grafting and tumor cell implantation in the adult CNS. Exp Neurol. 1998; 154:57–65. [PubMed: 9875268]

Kuhrt H, Hartig W, Grimm D, Faude F, Kasper M, Reichenbach A. Changes in CD44 and ApoE immunoreactivities due to retinal pathology of man and rat. J Hirnforsch. 1997; 38:223–229. [PubMed: 9176734]

Kwok A, Lai TY, Yuen KS. Epiretinal membrane surgery with or without internal limiting membrane peeling. Clinical & experimental ophthalmology. 2005; 33:379–385. [PubMed: 16033350]

Lee JE, Liang KJ, Fariss RN, Wong WT. Ex vivo dynamic imaging of retinal microglia using time-lapse confocal microscopy. Invest Ophthalmol Vis Sci. 2008; 49:4169–4176. [PubMed: 18487378]

Lee SJ, Lee CS, Koh HJ. Posterior vitreomacular adhesion and risk of exudative age-related macular degeneration: paired eye study. American journal of ophthalmology. 2009; 147:621–626. e621. [PubMed: 19159862]

Lewis GP, Fisher SK. Up-regulation of glial fibrillary acidic protein in response to retinal injury: its potential role in glial remodeling and a comparison to vimentin expression. International review of cytology. 2003; 230:263–290. [PubMed: 14692684]

Lewis GP, Guerin CJ, Anderson DH, Matsumoto B, Fisher SK. Rapid changes in the expression of glial cell proteins caused by experimental retinal detachment. American journal of ophthalmology. 1994; 118:368–376. [PubMed: 7916177]

McLeod DS, Lefer DJ, Merges C, Lutty GA. Enhanced expression of intracellular adhesion molecule-1 and P-selectin in the diabetic human retina and choroid. Am J Pathol. 1995; 147:642–653. [PubMed: 7545873]

Mojana F, Cheng L, Bartsch DU, Silva GA, Kozak I, Nigam N, Freeman WR. The role of abnormal vitreomacular adhesion in age-related macular degeneration: spectral optical coherence tomography and surgical results. American journal of ophthalmology. 2008; 146:218–227. [PubMed: 18538742]

Pedler C. The Inner Limiting Membrane of the Retina. Br J Ophthalmol. 1961; 45:423–438. [PubMed: 18170691]

Provis JM, Sandercoe T, Hendrickson AE. Astrocytes and blood vessels define the foveal rim during primate retinal development. Invest Ophthalmol Vis Sci. 2000; 41:2827–2836. [PubMed: 10967034]

Ramirez JM, Ramirez AI, Salazar JJ, de Hoz R, Trivino A. Changes of astrocytes in retinal ageing and age-related macular degeneration. Exp Eye Res. 2001; 73:601–615. [PubMed: 11747361]

Reichenbach A, Bringmann A. New functions of Muller cells. Glia. 2013; 61:651–678. [PubMed: 23440929]

Schachtrup C, Ryu JK, Helmrick MJ, Vagena E, Galanakis DK, Degen JL, Margolis RU, Akassoglou K. Fibrinogen triggers astrocyte scar formation by promoting the availability of active TGF-beta after vascular damage. J Neurosci. 2010; 30:5843–5854. [PubMed: 20427645]

Sebag, J. The Vitreous: Structure, Function and Pathobiology. Springer-Verlag; 1989.

Sebag J. Anatomy and pathology of the vitreo-retinal interface. Eye. 1992; 6(Pt 6):541–552. [PubMed: 1289128]

Seddon JM, Sharma S, Adelman RA. Evaluation of the clinical age-related maculopathy staging system. Ophthalmology. 2006; 113:260–266. [PubMed: 16458093]

Sethi CS, Lewis GP, Fisher SK, Leitner WP, Mann DL, Luthert PJ, Charteris DG. Glial remodeling and neural plasticity in human retinal detachment with proliferative vitreoretinopathy. Invest Ophthalmol Vis Sci. 2005; 46:329–342. [PubMed: 15623793]

Spencer LM, Foos RY. Paravascular vitreoretinal attachments. Role in retinal tears. Arch Ophthalmol. 1970; 84:557–564. [PubMed: 5478879]

Suk K. Unexpected role of lipocalin-type prostaglandin D synthase in brain: regulation of glial cell migration and morphology. Cell Adh Migr. 2012; 6:160–163. [PubMed: 22568990]

Sullivan R, Penfold P, Pow DV. Neuronal migration and glial remodeling in degenerating retinas of aged rats and in nonneovascular AMD. Invest Ophthalmol Vis Sci. 2003; 44:856–865. [PubMed: 12556422]

Wang M, Wang X, Zhao L, Ma W, Rodriguez IR, Fariss RN, Wong WT. Macroglia-microglia interactions via TSPO signaling regulates microglial activation in the mouse retina. J Neurosci. 2014; 34:3793–3806. [PubMed: 24599476]

Wang MY, Nguyen D, Hindoyan N, Sadun AA, Sebag J. Vitreo-papillary adhesion in macular hole and macular pucker. Retina. 2009; 29:644–650. [PubMed: 19357556]

Wiznia RA. Posterior vitreous detachment and idiopathic preretinal macular gliosis. American journal of ophthalmology. 1986; 102:196–198. [PubMed: 3740180]

Wong WT. Microglial aging in the healthy CNS: phenotypes, drivers, and rejuvenation. Frontiers in cellular neuroscience. 2013; 7:22. [PubMed: 23493481]

Wu KH, Madigan MC, Billson FA, Penfold PL. Differential expression of GFAP in early v late AMD: a quantitative analysis. Br J Ophthalmol. 2003; 87:1159–1166. [PubMed: 12928288]

Yoshida M, Kishi S. Pathogenesis of macular hole recurrence and its prevention by internal limiting membrane peeling. Retina. 2007; 27:169–173. [PubMed: 17290198]

Highlights

- Glial cells extend through the ILM onto the vitreoretinal surface in all aged humans.
- Müller cells exit the retina ahead of astrocytes.
- There is an increase in preretinal glial membranes in retinas with choroidal neovascularization.
- Most preretinal glia are subclinical but could be precursors to larger epiretinal membranes.

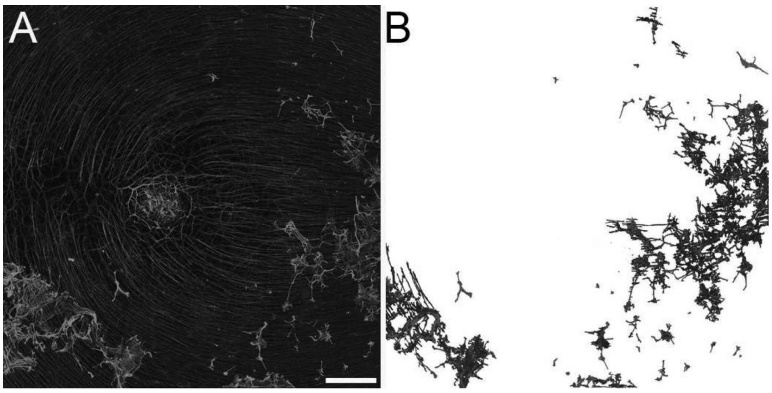

Figure 1. Quantification of GFAP-positive processes/cells on the vitreoretinal surface

(A) Retinas were labelled with GFAP and tiled 5x5 confocal Z stacks were collected at 10x to generate a map of each retinal region. (B) A new image was created after selecting $GFAP^+$ processes/cells on the vitreoretinal surface. Scale bar indicates: 500 μm.

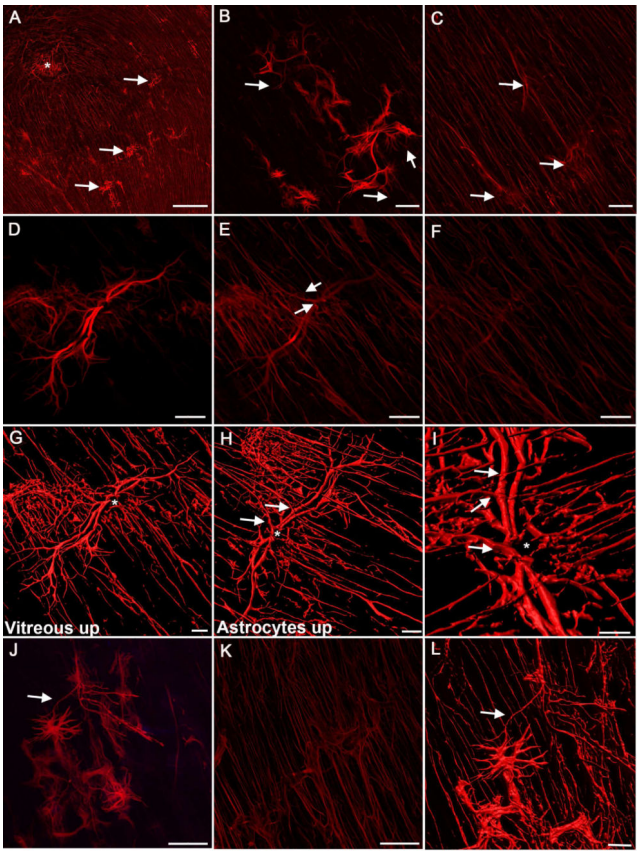

Figure 2. Glial sprouts were the simplest glial structures observed on the vitreal surface of the ILM

Retinas were labelled with anti-GFAP. (A) A low magnification tiled image of a posterior pole containing numerous focal glial sprouts (arrows), the fovea is shown with an asterisk. (B) At higher magnification, a Z stack slice demonstrates that glial sprouts lie in a focal plane above retinal astrocytes. Numerous branching processes from these cells extend into the retina below (arrows). (C) In the retina below, the astrocyte pattern is normal with the exception of tangled stalks where cells have exited the retina (arrows). (D) Closer investigation of a glial sprout demonstrates the length of processes. (E) Connections to cells within the retina are visible in the focal plane below “D” (arrows). (F) The overall astrocyte pattern below this sprout is normal. (G) A 3-D rendering of the same sprout demonstrates the main stalk (asterisk). Processes on the vitreal surface extend radially along the retinal surface. (H) When the opposing view of this 3-D image is examined, with the normal astrocyte pattern facing up and the sprout below, numerous connections are observed between the retinal astrocytes and the sprout (arrows). (I) Closer investigation provides better visualization of these connections (arrows) as well as the primary stalk (asterisk). (J) Some sprouts had a more stellate morphology extending numerous processes. Sprouts often joined together (arrow). (K) In the focal plane below, astrocytes within the retina were normal in density and pattern. (L) 3-D rendering of this glial sprout better demonstrates the connections between two sprouts by a fine process (arrow) as well as to astrocytes within the retina. Scale bars indicate: A: 500 μm, B-F, J, K: 50 μm and G-I, L: 20 μm.

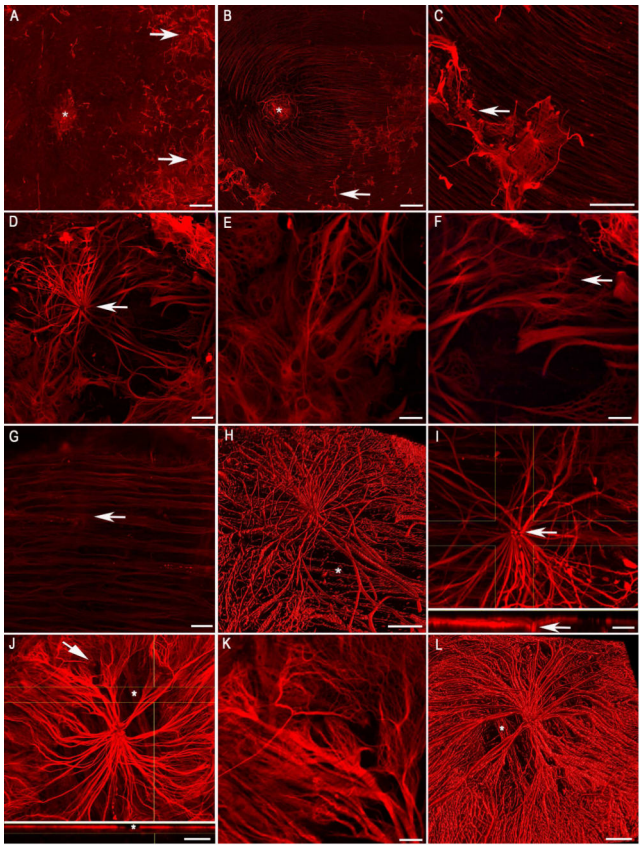

Figure 3. Multiple GFAP-positive cells exited the retina through one point to create glial blooms

Retinas stained with anti-GFAP are shown. (A, B) Low magnification tiled images showing posterior pole regions containing glial blooms (arrows). An asterisk indicates the fovea. (C) Higher magnification of two glial blooms joined by fine processes (arrow). (D) A glial bloom at high magnification shows multiple stalks exiting from one site in the retina (arrow). (E) In some cases, thick processes terminated as arborizations, creating a net-like appearance. (F) In others, stalks branched into multiple long fine processes (arrow). (G) The astrocytes in the retina below have a normal pattern with only a focal disruption where cells exited the retina (arrow). (H) Three dimensional rendering further demonstrates that this bloom lies above the normal astrocyte layer (asterisk). (I) The exit of glial processes from the retina (arrow) is evident in the cross section rendering. (J) Another example of a glial bloom is shown along with the cross sectional view demonstrating the bright GFAP labeling above the retina. An asterisk indicates an area without glial cells on the vitreoretinal surface where retinal astrocytes are visible. (K) The arborizations of the thick glial processes shown by the arrow in “J” are shown at higher magnification. (L) Three dimensional rendering of a bloom shows the layer of astrocytes below (asterisk). Scale bars indicate: A, B: 500 μm; C, D, G, H, J, L: 50 μm; E, F, I, K: 20 μm.

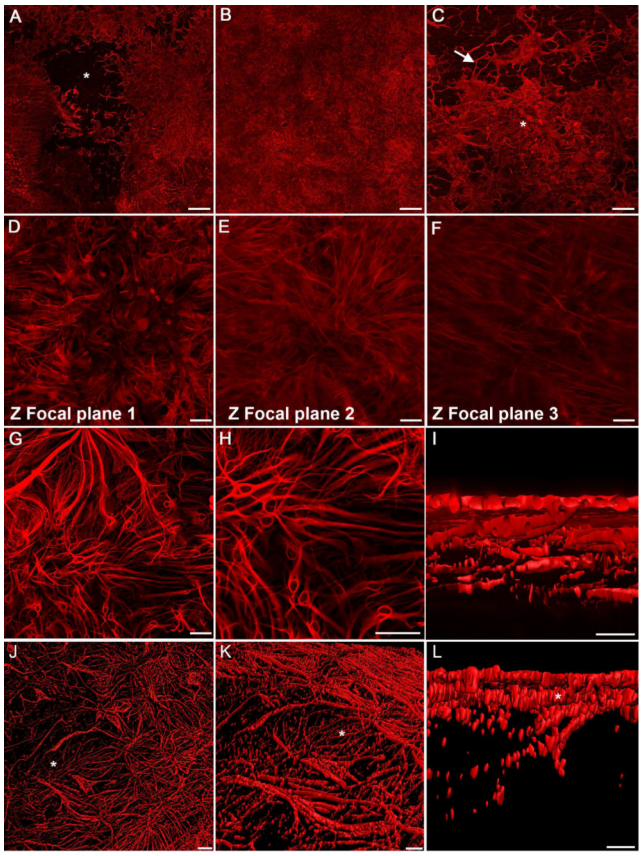

Figure 4. Multiple glial blooms coalesced to form continuous glial membranes

GFAP labeling of wholemount retinas demonstrates large glial membranes. (A) This tiled image of a posterior pole shows two large membranes merging above a normal astrocyte pattern (asterisk). (B) A continuous glial membrane covers the entire area of this tiled imaged. (C) Connections between blooms (arrow) create this larger glial membrane (asterisk). (D) Higher magnification demonstrates the density of these structures. (E) In the focal plane below "D", numerous $GFAP^+$ processes are present. (F) Astrocytes in the retina below are tortuous with misaligned processes. (G) In another membrane, thick, $GFAP^+$ processes arborize into smaller processes which connect with one another. (H) Many smaller structures within this membrane appear to be individual cells. Long processes extend between these glial cells and into the retina. (I) A digital cross sectional view demonstrates the multiple layers of $GFAP^+$ cells. The connections between the top layer (which lies in the vitreous) and astrocytes below can be observed. (J) The complexity of membranes is also shown in this 3D rendering. The astrocytes in an area lacking membrane (asterisk) are visible. (K) A side view of this membrane shows the astrocyte layer below (asterisks). (L) A cross sectional view demonstrates the astrocytes (asterisk) below the glial membrane. Scale bars indicate: A-C: 500 μm; D-H: 50 μm; I: 10 μm, and J-L: 20 μm.

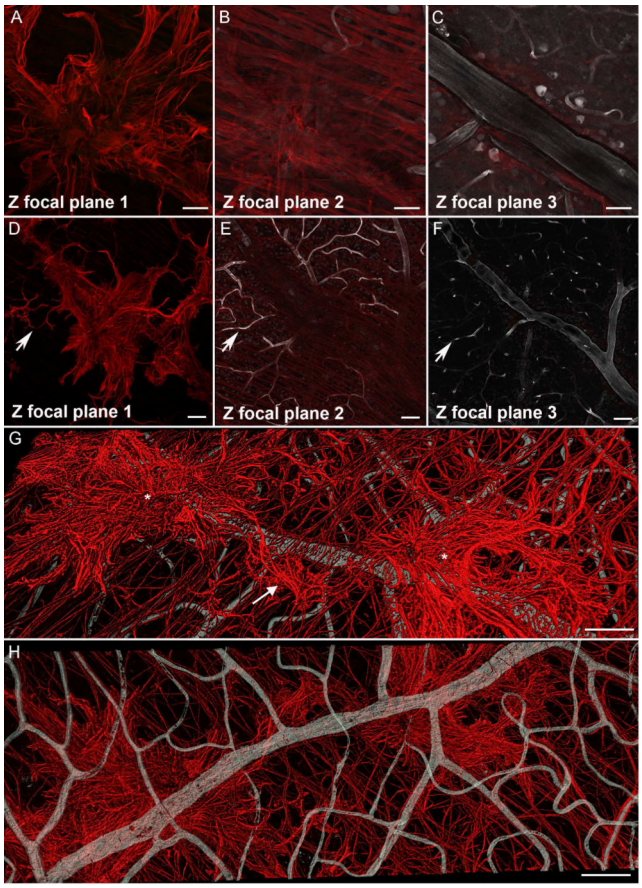

Figure 5. Preretinal glial structures were associated with retinal vessels

Retinal wholemounts shown were stained with anti-GFAP (red, glia) as well as UEA lectin (grey, blood vessels). (A-C) A glial sprout is shown extending onto the vitreal surface above a large vessel branch point. (D-F) Tiling of multiple images shows glial sprouts and blooms above retinal capillaries (arrow) as well as a larger vessel and branch point. (G) A 3D rendering of multiple glial blooms (asterisks) joined by a glial sprout (arrow) above a large retinal vessel. (H) The same 3D image viewed from the blood vessels side. Scale bars indicate: A-C: 50 μm; D-H: 100 μm.

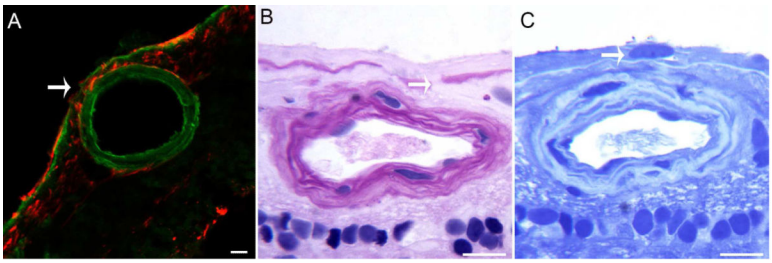

Figure 6. Glial cells exited the retina through breaks in the ILM

(A) Retinal wholemounts labeled for GFAP (red) were cryopreserved and sections stained for laminin (green) to label the ILM. $GFAP^{+}$ cells are observed in the vitreous adjacent to a break (arrow) in the ILM. (B) Breaks in the ILM (arrow) are evident in JB4-embedded regions of a retina stained with PAS and hematoxylin. (C) Nuclei (arrow) are visible on the vitreoretinal surface in sections stained with toluidine blue. Scale bars indicate: A: 40 μm and B, C: 20 μm.

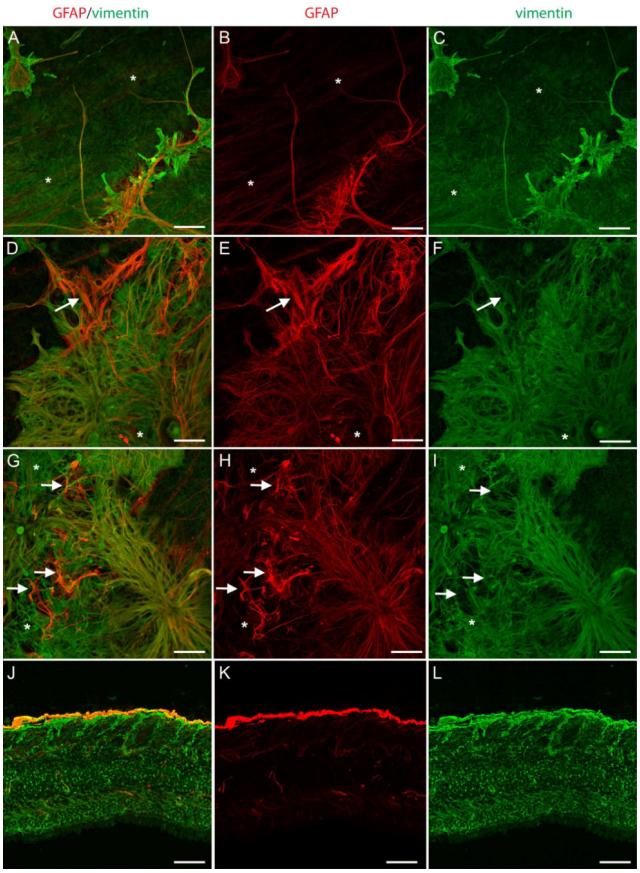

Figure 7. Retinal wholemounts stained for GFAP (red) and vimentin (green) demonstrate both Müller cells and astrocytes in preretinal glial structures

(A-C) GFAP$^+$ and vimentin$^+$ cells are observed in glial sprouts above a normal astrocyte template and Müller cell endfeet (asterisks). (D-I) In larger glial blooms and membranes, most cells are double-positive. Some cells/processes (arrow) have only GFAP while others (asterisk) have only vimentin. (J-L) A wholemount cross sectioned demonstrates staining of Müller cells with vimentin (green) and astrocytes with GFAP (red). Some lighter GFAP staining is seen in some Müller cells. The membrane above the Müller cell endfeet is double-positive. Scale bars indicate 40 μm.

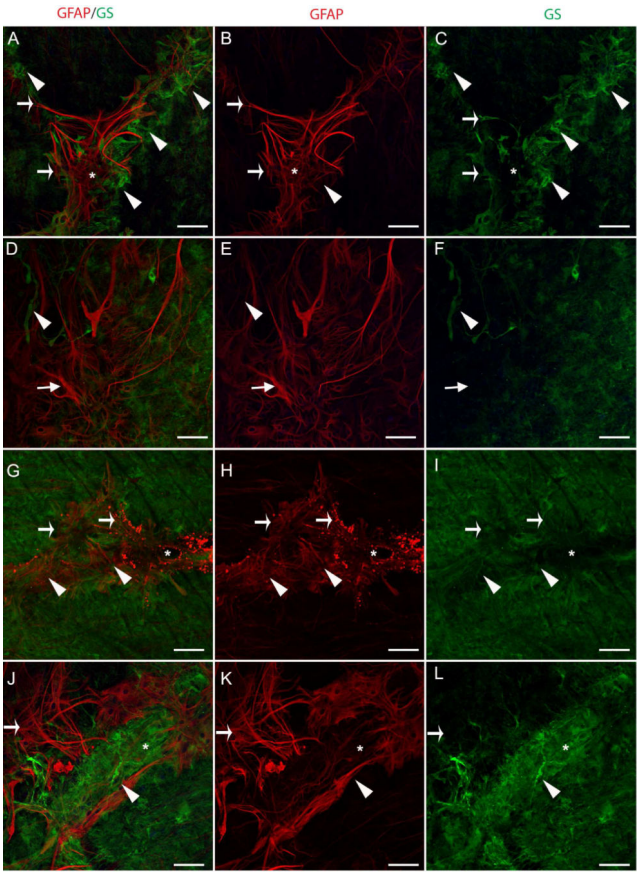

Figure 8. Retinal wholemounts labelled with GFAP (red) and GS (green) confirm two cell populations in preretinal glial structures

(A-C) Above a retinal vessel branch point (asterisk), glial sprouts contain GFAP and GS^{+} long processes that extend into the vitreous (arrows). $GFAP^{+}$, GS^{-} tangles are also observed (asterisk). In addition, intense GS staining (arrowhead) could indicate either swelling or aggregation of Müller cell endfeet at the ILM. (D-F) The glial bloom shown contains primarily $GFAP^{+}$, GS^{-} processes/cells (arrow) with a few $GFAP^{-}$, GS^{+} processes (arrowhead). (G-I) A glial sprout along a large retinal vessel (asterisk) contains double labelled processes/cells (arrowhead) as well as cells expressing only GFAP (arrows), which appears blebbed. (J-L) A dense area of GS^{+} cells (arrowhead) lies above a $GFAP^{+}$ glial bloom (arrow). Scale bars represent 40 μm.

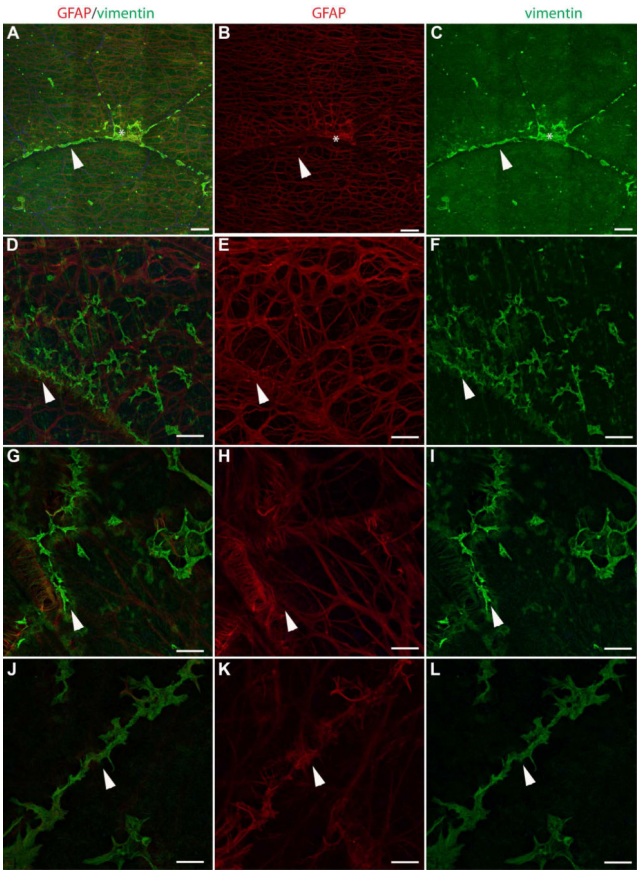

Figure 9. Müller cells exited the retina ahead of astrocytes

Retinal wholemounts stained for GFAP (red) and vimentin (green) are shown. (A-C) This area had no preretinal GFAP but contained vimentin^{+} sprouts (arrowhead). One small area (asterisk) had a tangle of GFAP^{+} processes. (D-F) Vimentin^{+} glial sprouts (arrowhead) are shown at higher magnification above a normal astrocyte pattern. (G-I) Under other areas of vimentin only sprouts (arrowhead), singular GFAP^{+} processes extended onto the vitreal side of the ILM. (J-L) Vimentin^{+} sprouts with a few GFAP^{+} processes (arrowhead) are shown in an area above a retinal vessel. Scale bar represent: A-C: 200 μm, D-L: 40 μm.

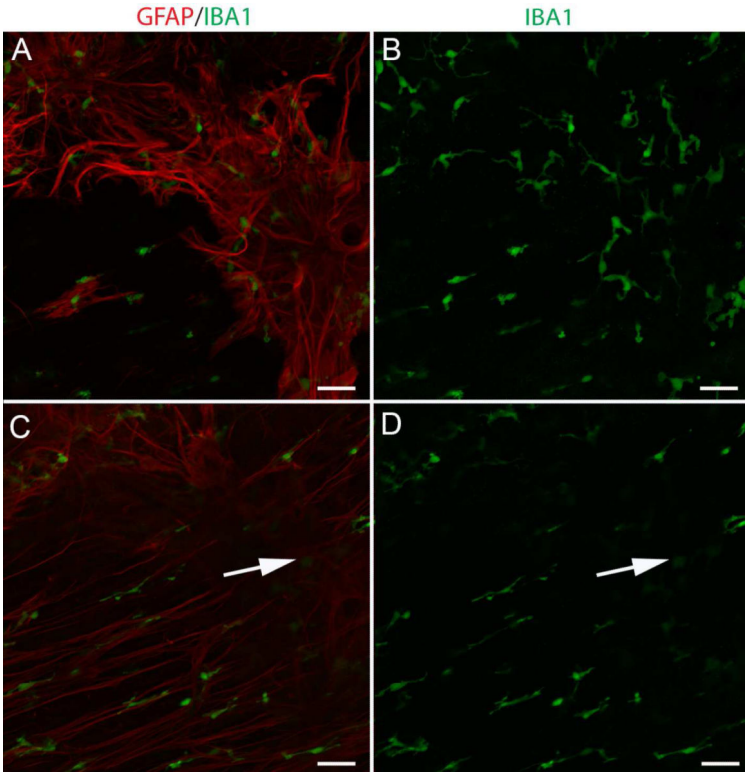

Figure 10. IBA-1 positive cells associated with glial cells on the vitreoretinal surface

Wholemount retinas labeled with anti-GFAP (red) and anti-IBA-1 (green). (A, B) IBA-1^{+} cells associate with glial sprouts and blooms. (C, D) These cells were not concentrated at the base where glia exited the retina (arrow). Scale bars indicate 50 μm.

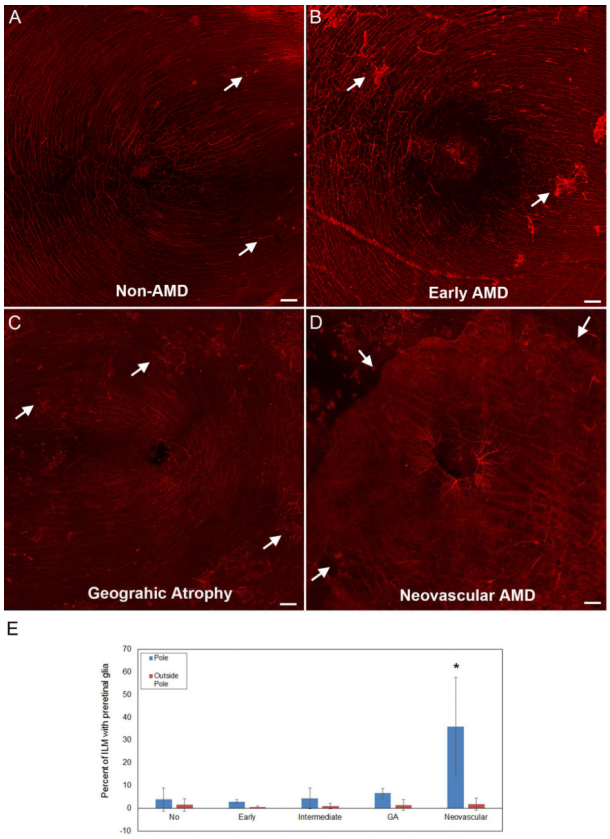

Figure 11. Large glial membranes were most prominent in neovascular AMD retinas

Retina wholemounts stained for GFAP (red) are shown. Tiled images taken at 10x are shown from representative (A) non-AMD retina, (B) early AMD, (C) geographic atrophy, and (D) neovascular AMD. In all images, arrows indicate some of the preretinal glia. Images were taken with the fovea centered. (E) Graphs show the average percentage of posterior pole tiled images covered with $GFAP^+$ cells on the vitreal surface. (F) Graphs show the average percentage of the ILM covered by preretinal $GFAP^+$ structures. As shown, there was a significant increase in the $GFAP^+$ cells on the vitreal side of the ILM in neovascular AMD in the posterior pole but not outside this area. Scale bars indicate 200 μm. Asterisks indicate significant difference compared to the non-AMD group.

Table 1

Donor eyes used in this study.

Donor ID	Age at death	Eye Used	AMD classification	AMD treatment	other ocular disease	Visual acuity	Pretinal glia: Posterior Pole	Preretinal glia: outside pole	Other medical problems	Cause of death
1	79	OS	non-AMD	No	None	NA	sprouts	sprouts		chronic pulmonary disease
2	94	OD	non-AMD	No	cataracts removed OU	20/25 (14)	blooms	blooms/sprouts	HTN, CHF, PVD, AF	cardiogenic shock
3	80	OD	non-AMD	No	none	NA	sprouts	no	cardiovascular disorder,	coronary disease
4	87	OS	non-AMD	No	cataracts removed OU	20/40 (8)	sprouts	blooms	HTN, HC, DM (II), heart attack	CHF
5	73	OU	non-AMD	No	cataracts removed OU	NA	blooms/membrane	blooms/membrane	HTN	CHF
6	64	OS	non-AMD	No	none	NA	sprouts	nothing		unknown
7	91	OD	non-AMD	No	BRVO macular edema, cataracts removed OU	20/20 (26)	sprouts	sprouts	HTN, DM, HC	Complete heart block
8	84	OU	non-AMD	No	Yag laser (2006), cataracts removed OU, laser	NA	sprouts	sprouts	AD, HTN, borderline DM	cardiac arrest
9	91	OS	early	No	cataracts removed OU glaucoma-laser surgery	20/80 (12)	sprouts/blooms	sprouts	PVD	HF and AF
10	86	OU	early	No	cataracts removed OU	20/25; 20/30 (37)	sprouts	sprouts	HC, dementia	Dementia/AD
11	97	OD	GA	No	cataracts removed OU	996 (8)	sprouts	sprouts	HTN, HC, PVD	spinal stenosis CHF
12	96	OD	GA	No	cataracts OU	996 (6)	blooms	blooms/sprouts		Respiratory failure/pneumonia
13	92	OD	GA	No	cataracts OU	20/40 (27)	blooms	blooms	HTN, HC	CHF
14	87	OD	intermediate	No	cataracts OU	20/30 (3)	sprouts	blooms	HTN, AF	Internal bleeding
15	92	OS	intermediate	No	retinal embolus, cataracts removed OU	20/30 (12)	blooms	blooms	HC, CHF, PVD, HTN	CHF
16	86	OS	intermediate	No	cataracts removed OU	NA	blooms/membrane	blooms/membrane		unknown
17	90	OD	intermediate	No	cataracts removed OU	20/30 (17)	sprouts	sprouts	HTN, CHF, AF	CHF, CA, hypoxic respiratory failure, renal failure, pulmonary HTN
18	84	OS	intermediate	No	cataracts removed OU	20/30 (9)	sprouts	nothing	HTN, heart attack	influenza/pneumonia
19	100	OS	neovascular	PDT	Glaucoma	20/400 (17)	blooms/membranes	sprouts	HTN, HC	HF
20	85	OS	neovascular	ranibizumab	cataracts removed OU	996 (8)	membranes	sprouts	HTN	esophageal cancer
21	97	OS	neovascular	diode laser	cataracts removed OU	996 (78)	large scar: couldn't image pole	blooms/sprouts	HTN, CHF	lung cancer- metastases to adrenal glands
22	86	OS	neovascular	No for AMD, laser for glaucoma	glaucoma, ERM OS, subretinal hemorrhage	20/60 (6)	membranes	blooms/sprouts	DM (II), AF, Parkinson's	Acute Respiratory Failure

Donor ID	Age at death	Eye Used	AMD classification	AMD treatment	other ocular disease	Visual acuity	Pretinal glia: Posterior Pole	Preretinal glia: outside pole	Other medical problems	Cause of death
23	96	OD	neovascular	possible laser	cataracts removed OU	996 (5)	membranes	blooms/sprouts	HTN, DM, HC, heart attack	Unknown
24	94	OD	neovascular	PDT	cataracts removed OU	20/25 (2)	membrane	sprouts	HTN, Parkinson's disease	CVA
25	78	OU	neovascular	21 ranibizumab injections OD, laser OD at border	ERM OD, retinal tears-laser cataracts removed OU	20/60; 996 (4)	membranes	membrane	HTN, DM, HC	pulmonary embolism
26	95	OD	neovascular	bevacizumab	glaucoma OU, ERM	998 (4)	membranes	blooms/sprouts	HTN	CVA
27	81	OS	neovascular	Focal laser	Glaucoma	20/400 (1)	blooms/membranes	sprouts	HTN, DM	Liver Disease
16B	86	OD	neovascular	No	cataracts removed OU	NA	blooms/membrane	blooms/membrane		unknown
28	102	OD	neovascular	No	cataracts removed OU	997 (5)	blooms/membranes	blooms/sprouts	HTN	CHF

This list includes available data regarding ocular and systemic diseases of donors. The preretinal glial structures observed in each are also noted. Abbreviations include: AD-Alzheimer's disease, AF-atrial fibrillation, AMD-age-related macular degeneration, BRVO-branch retinal vein occlusion, CA-cardiac arrest, CHF-congestive heart failure, CVA-cerebrovascular accident, DM-diabetes mellitus, ERM-epiretinal membrane, GA-geographic atrophy, HC- high cholesterol, HTN-hypertension, HC-high cholesterol, HF-heart failure, OD-oculus dexter, OS-oculus sinister, OU-oculus uterque, PDT-photodynamic therapy, PVD-peripheral vascular disease. Visual acuity codes: NA: not available; 996: count fingers, 997: hand motion, 998 no light perception. The number of months since visual acuity was last scored is listed in parentheses.

Table 2

A list of antibodies used.

Antibody	Source/Catalog #	Dilution	Cells labeled
Ck-α-GFAP	Millipore ab5541	1:500	Astrocytes/activated Müller cells
Ck- α -vimentin	Millipore ab5733	1:500	Müller cells
Rb- α -vimentin	Abcam ab4539	1:300	Müller cells
Rb- α -IBA-1	Wako 019-19741	1:500	Microglia, hyalocytes
Ms- α -GFAP	Sigma G3893	1:500	Astrocytes & activated Müller cells
Ms- α -GS	Millipore MAB302	1:1000	Müller cells
Rb- α -laminin	Sigma L9393	1:500	ILM, blood vessels
FITC conjugated UEA lectin	Sigma L9006	1:100	Blood vessels
Gt-a-Chick cy3	JIR 103-165-155	1:200	
Gt-a-Chick 405	JIR 103-475-155	1:200	
Gt-a-Rb Alexafluor 647	Invitrogen A21244	1:200	
Gt-a-Mouse cy3	JIR 115-165-003	1:200	

Antibodies are listed along with source and dilution used. Abbreviations include: Ck: chicken, Gt: Goat, Rb: Rabbit; Ms: Mouse, JIR-Jackson Immunoresearch